Research Square

Preprints are preliminary reports that have not undergone peer review.
They should not be considered conclusive, used to inform clinical practice,
or referenced by the media as validated information.

Microalloying-enabled hierarchical reconstruction of Bi-phase for strain resilience improvement and high strength-ductility synergy of Sn–Bi solder alloys

Peng Wu
Harbin Institute of Technology
Ruyu Tian
Harbin Institute of Technology
Tao Deng
Zhengzhou Advanced Research Institute, Harbin Institute of Technology
Shuhan Dong
Harbin Institute of Technology
Xiaoliang Ji
Beijing University of Technology
Jianchao Liang
Harbin Institute of Technology
Baolei Liu
Harbin Institute of Technology
Yanhong Tian
tianyh@hit.edu.cn

Harbin Institute of Technology

Research Article

Keywords:

Posted Date: October 28th, 2026

DOI: https://doi.org/10.21203/rs.3.rs-10066115/v1

License: This work is licensed under a Creative Commons Attribution 4.0 International License.
Read Full License

Additional Declarations: No competing interests reported.

Microalloying-enabled hierarchical reconstruction of Bi-phase for strain resilience improvement and high strength-ductility synergy of Sn–Bi solder alloys

Peng Wu [a, b], Ruyu Tian [a, b*], Tao Deng [b], Shuhan Dong[a], Xiaoliang Ji[c], Jianchao Liang [a, b], Baolei Liu [a, b], Yanhong Tian [a, b*]

a State Key Laboratory of Precision Welding & Joining of Materials and Structures, Harbin Institute of Technology, Harbin 150001, China.

b Zhengzhou Advanced Research Institute, Harbin Institute of Technology, Zhengzhou 45000, China

c College of Materials Science and Engineering, Beijing University of Technology, Beijing 100124, China

Email: tianry@hit.edu.cn, tianyh@hit.edu.cn.

Abstract: In this work, we report a trace Cr/V microalloying strategy that reconstructs the Bi-rich constituent in Sn–Bi solder alloys, achieving a total elongation of 61.64% and an ultimate tensile strength of 79.64 MPa, representing increases of 72.26% and 26.00%, respectively, over the unmodified alloy. The addition of alloying elements alters the interfacial thermodynamics and diffusion kinetics of the Sn-Bi system, thereby changing the solidification pathway, refining the eutectic structure at the mesoscopic scale, and introducing microscale substructures such as abundant dislocation walls, low-angle grain boundaries, and twins, as well as nanoscale Sn-rich regions, within the Bi-rich phase. These hierarchical structural features change the role of the Bi-rich phase during deformation. The reconstructed Bi-rich constituent no longer serves as a weak region for rapid crack propagation, but instead accommodates

strain resilience through more dispersed and constrained microcrack activity. This, in turn, improves the deformation compatibility between the Sn-rich and Bi-rich phases. Multiscale calculations further show that the refined microstructure and distributed microcracking alleviate local stress concentration and delay the rapid development of macroscopic cracks. This work reveals a new mechanism about the brittle Bi-rich phase participates in deformation and damage evolution in Sn–Bi eutectic solder alloy, and provides a general design strategy for improving the mechanical reliability of eutectic alloys through internal structural modification of intrinsic brittle phases.

1. Introduction

The rapid development of consumer electronics has driven the industry toward advanced packaging[1,2]. In electronic packaging, a lower soldering temperature results in lower thermal stress and fewer defects, such as warpage during assembly, and also allows for the use of lower-cost substrates[3]. The low-melting-point Sn–Bi eutectic alloy has attracted widespread attention[4] for temperature-sensitive devices[5] in advanced electronic packaging due to its favorable melting point[6] and relatively high strength[7]. However, its brittle fracture behavior and poor ductility at room temperature[8] severely limit its widespread application[9], particularly in terms of drop impact resistance in end-user devices[10–12]. Liu et al.[13] found that crack propagation during drop failure is closely related to the fracture toughness of the solder; reducing the crack tip strength can alter the crack propagation path, thereby effectively retarding crack growth. Fowler et al.[14] proposed that improving the ductility of solder alloys can effectively enhance their drop impact resistance. It is generally accepted Microstructural failure in these solder joints typically originates from the poor cooperative deformation ability between the β-Sn matrix and the Bi phase[12,15–17]. Cai et al.[18], through in-situ tensile Scanning Electron Microscope (SEM) observations, found that crack initiation and propagation preferentially occur at the phase boundaries, and the inherent brittleness of the Bi phase governs the macroscopic mechanical response of the alloy.

Previous efforts to improve the mechanical performance of Sn–Bi alloys have

primarily focused on microstructural refinement, dispersion of secondary phases, or solid solution strengthening via microalloying additions. Adjusting the Bi content can fundamentally alter the distribution of the brittle phase, thereby effectively enhancing the ductility[19]. However, compositions that deviate excessively from the eutectic point will lead to an increase in the melting point and an uncontrollable melting range[20]. Another more widely adopted approach to property improvement is through microalloying. Elements such as Ag[21-24], In[25-28], Sb[29], Zn[30], Ni[31], and et al.[32-34] have been attempted to incorporate into Sn-Bi alloys. However, the addition of these elements preferentially reacts with Sn—either by forming solid solutions[23,25] or generating secondary phases[24,28]—resulting in an improvement in the shear strength[21-24,29-34] of the solder alloys.

Despite the effectiveness of these strategies in improving the strength of Sn–Bi alloys, they mainly focus on modifying the Sn-rich matrix or refining the eutectic microstructure, while the brittle Bi phase, which is the principal source of ductility loss, remains largely unaddressed. As a consequence, the intrinsic deformation and fracture behavior of the Bi phase are still poorly controlled. The difficulty of coordinated deformation between the ductile Sn phase and the brittle Bi phase remains unresolved, leading to the poor strain resilience of the alloy. A key yet unexplored question is whether the mechanical behavior of the Bi phase can be directly tailored through alloy design. In this context, recent studies on eutectic high-entropy alloys offer an important clue. Pan et al.[35] achieved a synergistic improvement in strength and ductility by constructing a gradient structured hierarchical architecture, whereas Shi et al.[36]

enhanced the plasticity of eutectic high-entropy alloys through the introduction of hierarchical cracks. These results demonstrate that hierarchical structural design can effectively regulate local deformation and crack evolution, thereby overcoming the strength-ductility trade-off. Nevertheless, such a strategy has rarely been explored in Sn–Bi-based solder alloys.

Inspired by these studies, the present work proposes a Bi-phase-oriented microalloying strategy to designedly construct hierarchical structural features in the Bi phase. The selection of alloying elements was based on literature evidence and considerations of solid solubility, secondary-phase formation tendency, and electronegativity, among others. Cr and V were therefore chosen as candidate solutes with the aim of promoting their incorporation into the Bi phase and inducing local structural heterogeneity. More importantly, this design is expected to activate microcrack-mediated strain accommodation during deformation, thereby overcoming the intrinsic brittleness of the Bi phase and improving strain resilience without sacrificing strength. To verify this concept, the phase constitution, structural characteristics, deformation behavior, and mechanical properties of Cr and V microalloyed Sn–Bi alloys were investigated by combining transmission electron microscopy (TEM), double spherical aberration-corrected scanning transmission electron microscopy (STEM) with energy-dispersive X-ray spectroscopy (EDS), geometric phase analysis (GPA), and in situ tensile SEM observations. The simulation approaches encompass density functional theory (DFT), phase-field modeling (PFM), and the finite element method (FEM). This work establishes a multiscale understanding

of how targeted solute design modifies the Bi phase and enables strength–ductility optimization in Sn–Bi-based solder alloys.

2. Experimental and computational methods

2.1. Alloy preparation and thermal processing

In the present study, Sn–Bi-based alloys were prepared in-house from high-purity tin, Bismuth, Chromium and Vanadium. The alloying elements Cr and V were introduced as minor additions (concentration ≤ 0.3 wt.%) to ensure solid-solution conditions. Ingots of 99.99% Sn, 99.99% Bi, 99.99% Cr and 99.99% V were melted in vacuum furnace at 1273 K for 2 h, and then cooled down to room temperature in air. To obtain a microstructure approximating the reflowed condition, the ingots were remelted at 250 °C and subsequently cast into a preheated carbon mold. In this report, for convenience, the composition with the best mechanical properties, 50Sn49.795Bi0.2Cr0.005V (wt. %), is denoted as SBCV.

2.2. Microstructural characterization

microstructures were characterized via Electron Back Scatter Diffraction(EBSD, GeminiSEM 560, Carl Zeiss Microscopy GmbH, Germany) and field emission scanning electron microscopy. Prior to scanning, the samples were mechanically polished, followed by vibratory polishing to remove the surface deformation layer. EBSD data wes analyzed using the commercial software Aztec Crystal to determine the grain size distribution, grain boundary misorientation, and the fraction of low-angle grain boundaries (2°–15°).

TEM and high-resolution TEM (HRTEM) observations were performed using a Talos F200X transmission electron microscope (Thermo Fisher Scientific, USA) operated at an acceleration voltage of 30 kV. Thin alloy foils were prepared by mechanical thinning followed by either ion beam thinning or focused ion beam (FIB) milling. Low-angle grain boundaries, dislocation walls, and Bi grain boundaries within the Bi phase were examined in detail. Spherical aberration-corrected scanning transmission electron microscopy (Cs-corrected TEM) imaging was conducted on a double Cs-corrected ARM300F microscope (JEOL, Japan) operated at 300 kV, equipped with a dual silicon drift detector (SDD) for EDS. Elemental mapping was performed to determine the spatial distribution of Sn, Bi, Cr, and V within the Bi phase. GPA was carried out on HRTEM images using Digital Micrograph software (Gatan, USA) to quantify the local strain fields associated with deformation substructures and Sn-enriched regions.

2.3. Micromechanical testing and in situ tracking

Uniaxial tensile testing was conducted at room temperature on dog-bone specimens machined parallel to the casting direction. An initial strain rate of approximately 5×10^{-3} s^{-1} was applied using a universal testing frame. To ensure statistical reliability, a minimum of three identical specimens were tested per composition.

To capture the real-time dynamics of damage nucleation and crack path evolution, in situ tensile loading was performed directly inside the SEM chamber using a custom micromechanical stage. The loading was periodically paused to record high-resolution

images of the evolving strain localizations and crack deflections.

2.4. First-principles calculations

To further understand the influence of trace Cr and V solution on the solder alloys, the DFT calculations were conducted via the Cambridge Sequential Total Energy Package (CASTEP) code within the Materials Studio package. The electron-ion interactions were described using ultrasoft pseudopotentials, and the exchange-correlation functional was treated within the generalized gradient approximation (GGA). Sn/Bi interface supercells were constructed with and without Cr atomic substitutions. Interfacial energies were extracted following full ionic relaxation, with energy and force convergence thresholds rigorously set to ensure ground-state accuracy. A plane-wave cutoff energy of 500 eV was employed, and the Brillouin zone was sampled using a Monkhorst-Pack k-point mesh with a separation of 0.04 $Å^{-1}$. Geometry optimizations were performed until the forces on all atoms converged to less than 0.01 eV/Å.

2.5. Multiscale fracture simulations

Phase-field modeling was employed to simulate the trajectory and kinetics of crack propagation under different microstructural conditions. The governing equations coupled mechanical equilibrium with a phase-field damage variable, driven by local elastic strain energy density and intrinsic fracture toughness parameters derived from both literature benchmarks and our DFT outputs.

Finite element simulations were performed to investigate the stress distribution

under uniaxial tensile loading. Two-dimensional representative volume elements (RVEs) were constructed to represent the coarse eutectic regions and the refined lamellar structures, based on the actual microstructures observed via EBSD. The linear elastic properties of the Sn and Bi phases were assigned according to reported values. Stress concentration patterns and von Mises stress distributions were compared to evaluate the influence of microstructure on stress homogenization.

3 Results

3.1. Microstructure of solder alloy

EBSD mapping reveals a pronounced morphological transformation driven by the minor addition of Cr and V (Fig. 1). The SBCV alloy consists of a eutectic region and a β-Sn solid solution region. Compared with the Sn50Bi alloy, the addition of the microalloying elements Cr and V leads to a significant microstructural refinement of both the Sn and Bi phases. Specifically, this is manifested as a finer lamellar eutectic structure, as well as smaller and more uniformly distributed β-Sn solid solution regions. In contrast, in the eutectic Sn-Bi alloy, the Bi phase exhibits a relatively coarse lamellar or blocky morphology with limited substructure development. Grain size statistics further reveal that the grain size distributions of both the Sn and Bi phases in the SBCV alloy are shifted toward smaller values overall. The introduction of Cr and V substantially refines this classical eutectic architecture.

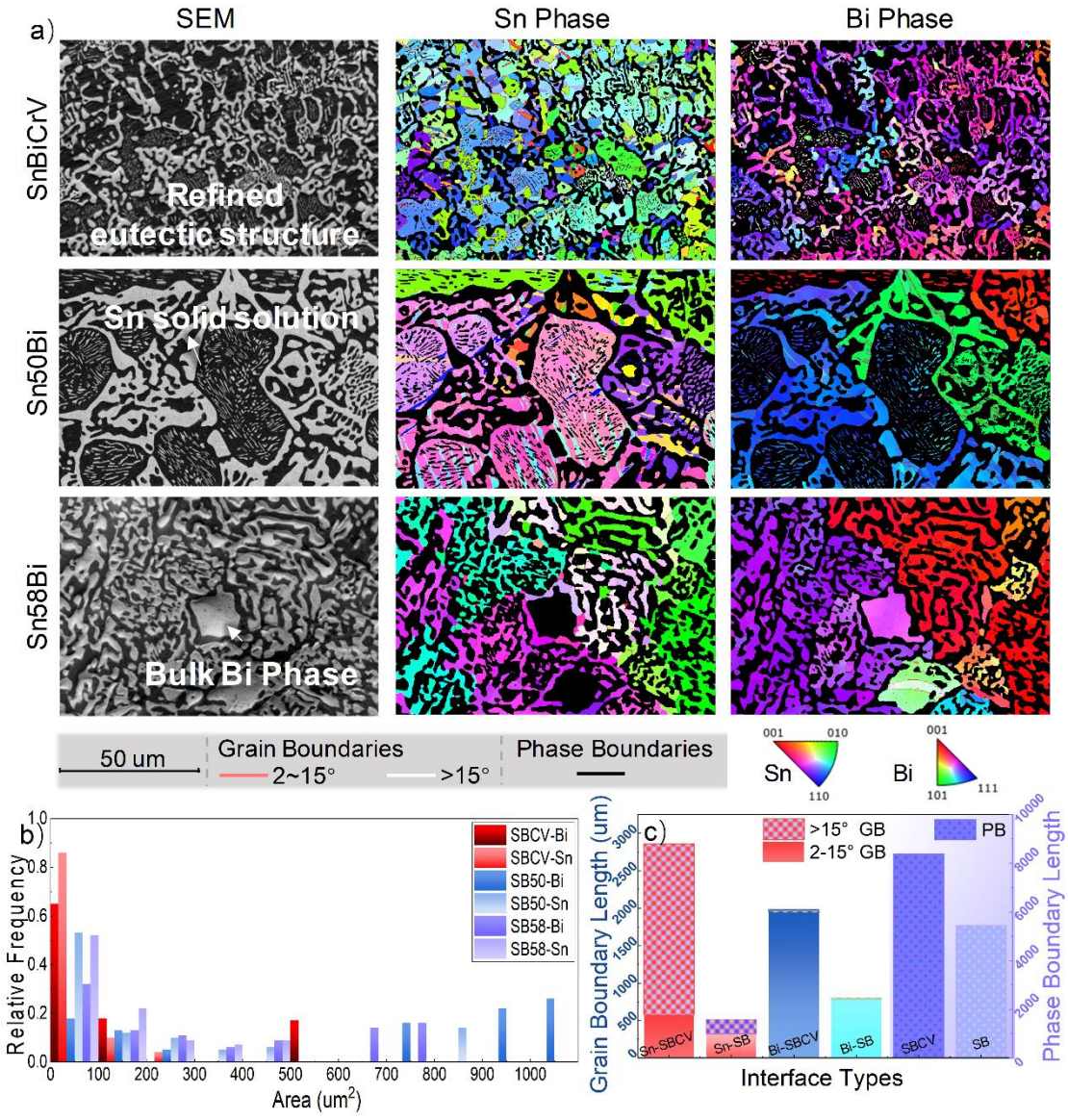


Figure 1. (a) SEM images and corresponding Inverse Pole Figure (IPF) maps of Sn58Bi, Sn50Bi, and SBCV alloys in the equiaxed zone; (b) grain size statistics of the alloys; (c) Statistical chart of grain boundary and phase boundary length in Sn58Bi alloy and SBCV alloy

The boundary characterization of SBCV and Sn-Bi solder alloys are summarized in Table 1. reveal a significant increase in the fraction of low-angle grain boundaries (LAGBs) within the Bi phase after microalloying. Notably, the phase in the SBCV alloys remains substantially finer and contains a higher LAGBs density. Specifically,

the phase boundary length and LAGBs length correspond to 1.5 to 2.26 times the values observed in the binary Sn-Bi alloys.

Table 1. Statistics for boundary characterization in the SBCR and Sn-Bi alloys

μm	PB	Sn-GB	Sn-LAGB	Sn-HAGB	Bi-GB	Bi-LAGB	Bi-HAGB
SB58	5437.6	510.9	309.4	201.5	802.3	777.9	24.4
SB50	6489.8	2119.9	152.4	1967.4	1436.3	1434.5	1.9
SBCV	7631.1	2856.8	553.6	2303.2	1980.1	1884.6	95.5

The microstructure of as-cast SBCV alloy was further analyzed by TEM. As shown in Fig. 2a, LAGBs subdivide the coarse Bi grains into subgrains with small misorientation angles, establishing a hierarchical internal structure. The inverse fast Fourier transform (IFFT) image in the inset of Fig. 2bconfirms that these boundaries consist of closely spaced, ordered dislocation arrays. Atomic strain fields around the LABGs are compared using the GPA in Fig. 2.c, revealing clear lattice distortion[37]. This indicates that the Bi lattice resides in a metastable state, characterized by internal stress concentrations. In addition, well-defined dislocation walls are observed[38], aligned along specific crystallographic vectors to accommodate local lattice rotations. Nanoscale twins frequently appear.

Taken together, in the SBCV alloy, a high density of deformation-related substructures, including LAGBs, dislocation walls, and twins, are observed within the Bi phase, which are rarely detected in the binary Sn-Bi alloy.

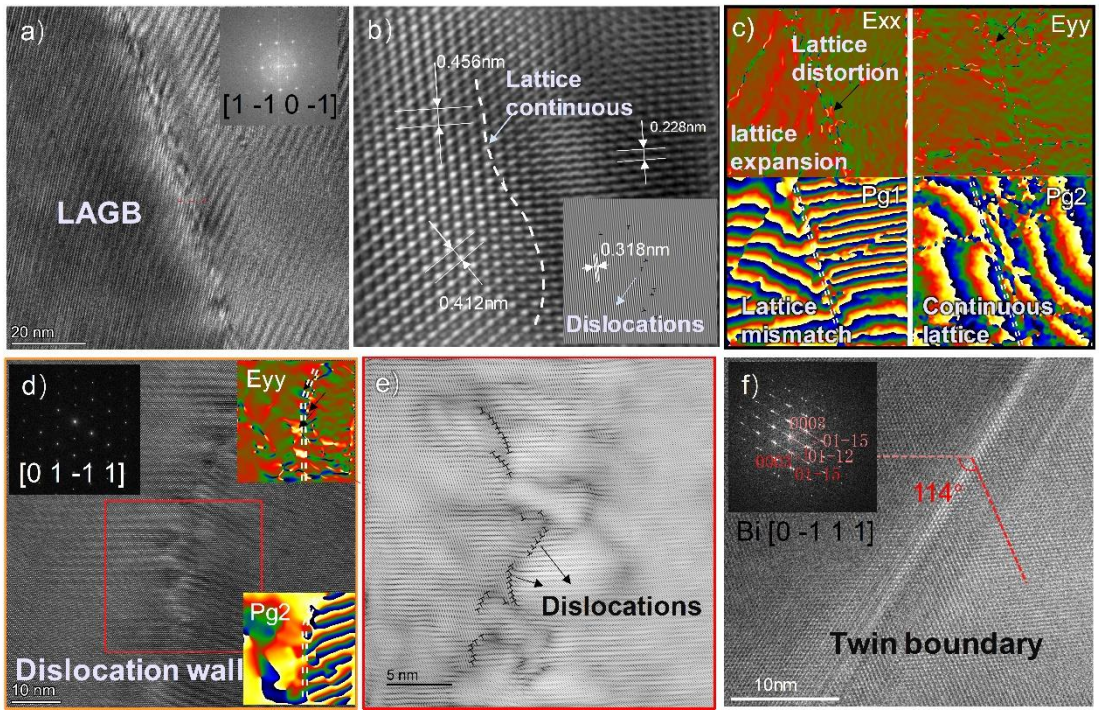


Figure 2. TEM images of Bi phase in the as-cast SBCV alloy. (a) HR-TEM image of LAGBs within the Bi phase. (b) HR-TEM image of local regions labelled by red box in (a), the inset showing the corresponding IFFT image in a single direction. (c) strain distribution around the LAGB , represented by ε_{xx} and ε_{yy}, respectively . (d) HR-TEM image of dislocation walls in the Bi phase of the SBCV alloy. Left inset: corresponding SAED pattern. Right inset: GPA εyy strain map of the interface. (e) IFFT of red box in (d) showing the dislocation walls in a single direction. (f) HR-TEM image of twin boundaries in the deformed Bi phase, left inset: corresponding SAED pattern

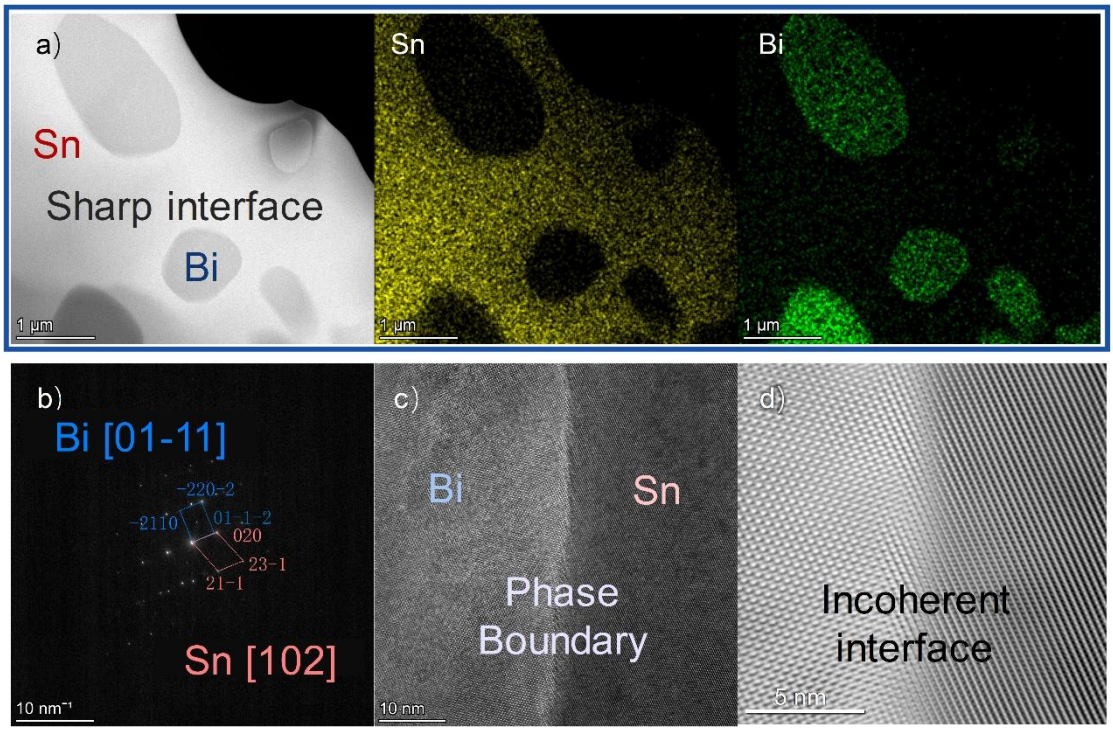


Figure 3. TEM images of the as-cast Sn-Bi alloy. (a) BF-TEM image and corresponding EDS maps; (b) SAED patterns of the Sn/Bi phase boundary. (c) HR-TEM image of the Sn/Bi phase boundary, and (d) the corresponding IFFT image

As presented in Bright-field transmission electron microscopy (BF-TEM) image and corresponding EDS maps of the as-cast Sn-Bi alloy (Fig. 3a), Sn-rich precipitates with characteristic sizes ranging from ~100 nm to 1 μm are frequently observed within the Bi phase, suggesting classical phase separation via nucleation and growth. These precipitates exhibit clear compositional contrast and distinct phase boundaries. Although certain interfaces appear to maintain an orientation relationship with the surrounding matrix (Fig. 3b), they remain delineated by distinct interphase boundaries.

In contrast, as shown in Fig. 4a-b, numerous special structures with characteristic dimensions of several tens of nanometers are detected within the Bi phase of the SBCV alloy. Importantly, BF-TEM images confirm that these regions exist within the

Bi grains and are densely distributed (Fig. 4a). Observations of individual regions (Fig. 4b) reveal that they exhibit a roughly circular or elliptical morphology. STEM-EDS mapping (Fig. 4c) further confirms local Sn enrichment within these nanoscale regions, whereas Cr and V remain uniformly distributed throughout the Bi lattice. Atomic-scale imaging using Cs-corrected TEM at the boundaries of the Sn-enriched regions (Fig. 4d) reveals that these regions share the same lattice structure as the matrix, with no detectable incoherent interfaces or secondary phase features. The corresponding IFFT image at the Sn-enriched region boundaries (Fig. 4e) shows a lattice mismatch of only half an atomic layer thickness, further demonstrating that the interior and exterior of the Sn-enriched regions maintain the same lattice structure without forming distinct interfaces. GPA analysis of the Sn-enriched regions reveals localized lattice strain fluctuations (Fig. 4f). The absence of sharp interfaces, together with the preserved lattice continuity with the Bi matrix, strongly suggests that these nanoscale Sn enrichments form via a spinodal decomposition process[39].

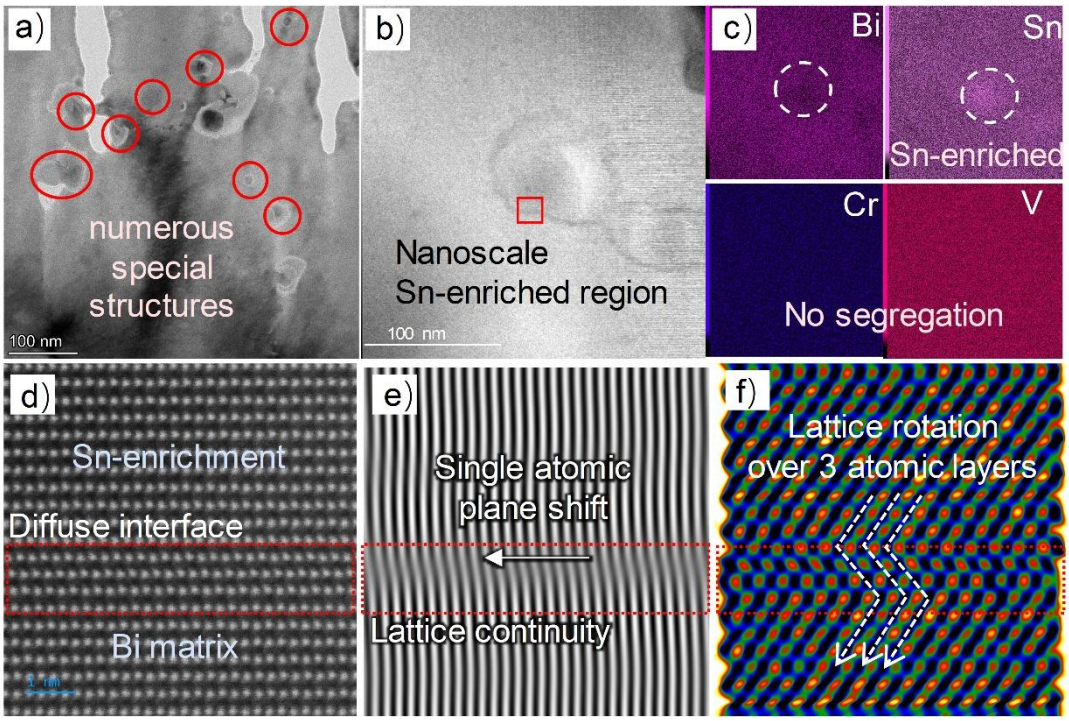


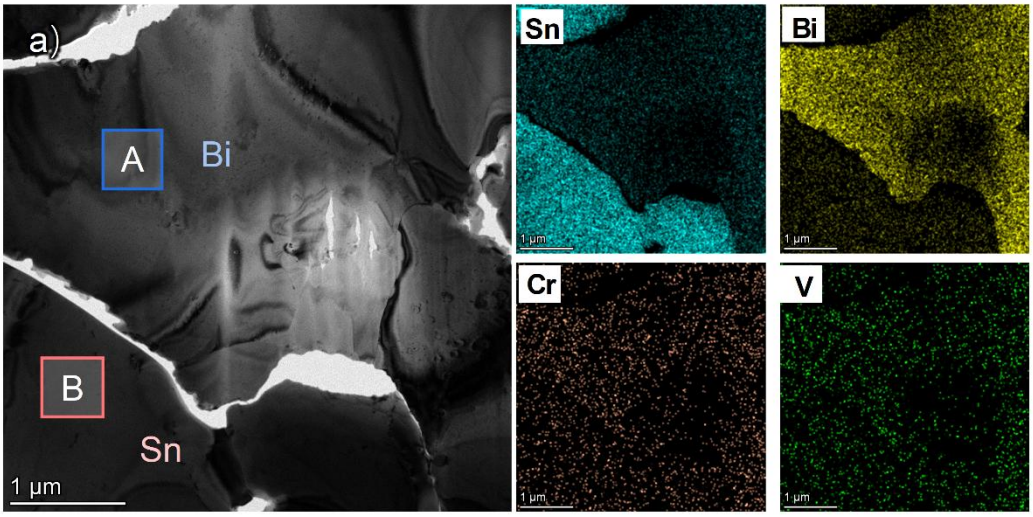
Figure 4. Characterization of Sn-enriched regions within the Bi phase in the SBCV alloy. (a,b) Bright-field TEM images of Sn-enriched regions. (c) STEM-EDS elemental mapping of the enriched region. (d) Cs-corrected TEM atomic-resolution image of the region labelled in (b), and (e) the corresponding IFFT image. (f) GPA strain map showing the εxx component

The distinct transition in transformation pathway—from coarse Sn precipitation in the binary alloy to nanoscale compositional modulation in the microalloyed alloy—indicates that the SBCV solid solution fundamentally alters both the thermodynamic landscape and the kinetic pathway of phase separation within the Bi phase[39].

3.2 Microalloying solid solution and microstructure formation mechanism

Elemental mapping reveals that Cr and V signals are dissolved to a certain extent within the Bi-rich regions, with no evidence of microalloying-induced elemental enrichment associated with secondary phase formation. The absence of new intermetallic compound (IMC) formation is further supported by the WDS results

acquired over a wider field of view (supporting information, Fig. S1). These findings are consistent with the uniform distribution of Cr and V within the Bi phase observed in Fig. 4c. Quantitative point EDS analysis of the Bi phase (Fig. 5b-c) further confirms the solid solution of Cr and V in the Bi phase, with concentrations of 4.75 at.% and 1.64 at.%, respectively.



b) Region A EDS analysis

	Atomic Fraction (%)	Atomic Error (%)
Sn	4.25	1.16
Bi	89.35	2.61
Cr	4.76	1.77
V	1.64	1.40

c) Region B EDS analysis

	Atomic Fraction (%)	Atomic Error (%)
Sn	96.28	0.57
Bi	2.65	0.34
Cr	0.72	0.21
V	0.34	0.18

Figure 5. Compositional characterization of the SBCV alloy. (a) BF-TEM image and corresponding STEM-EDS elemental maps of Bi, Sn, Cr, and V acquired from the same region. EDS analysis of region A (b) and B (c)

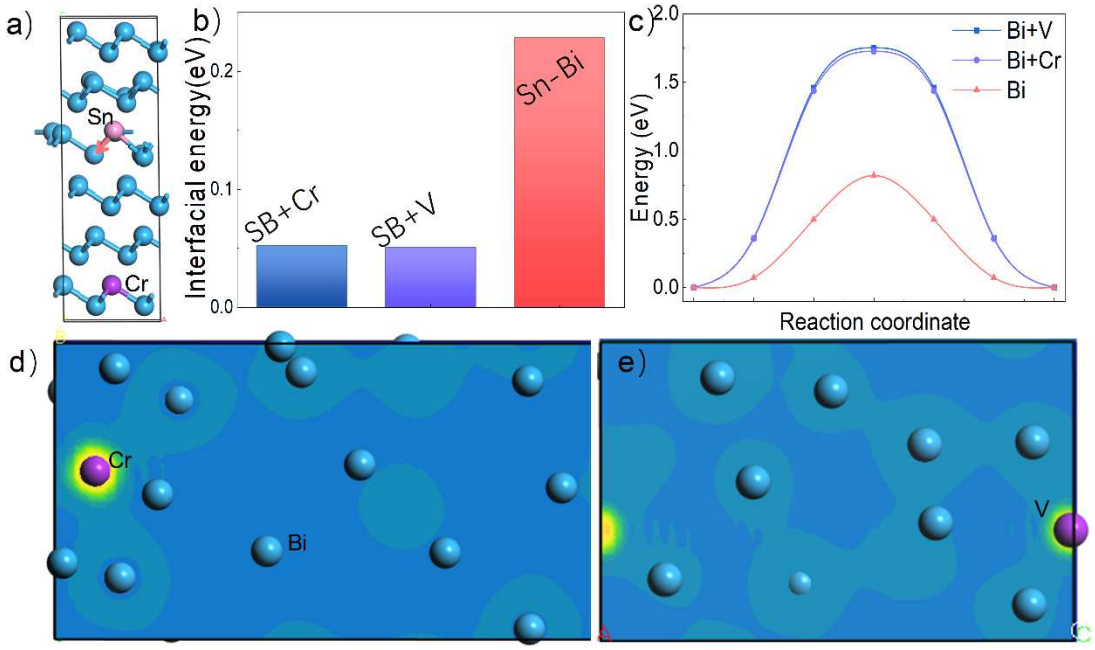


Figure 6. First-principles calculations of the effect of Cr/V solid solution on the Sn–Bi system. (a) Sn lattice with Cr and V dissolution. (b) Change in the Sn–Bi interfacial energy with Cr and V dissolution. (c) Diffusion barrier of Sn atoms in the Bi phase after Cr/V addition. (d,e) Charge density distribution of the Bi phase with Cr and V dissolution

To further understand the role of trace solute addition, first-principles calculations were performed to evaluate the interfacial energetics, atomic migration behavior, and electronic distribution of the modified system. The effects of Cr and V dissolution on the Bi phase were analyzed by first-principles calculations， and the results are shown in Fig. 6. The diffusion model used in the calculations is shown in Fig. 6a. As presented in Fig. 6b, the incorporation of Cr or V leads to a significant reduction in the Sn/Bi interfacial energy, from 0.222 eV in the undoped structure to 0.052 eV and 0.051 eV, respectively, indicating a substantial change in the local interfacial thermodynamic state upon solute addition. Meanwhile, the calculated migration barrier increases from 0.816 eV in the binary structure to 1.726 eV and 1.752 eV for the Cr- and V-containing models,

respectively (Fig. 6c), suggesting that the diffusion of Sn atoms in the Bi phase becomes considerably more difficult in the presence of these solutes. Fig. 6d has shown the total charge density distribution of the Cr-substituted configuration, which shows clear charge accumulation in the vicinity of the solute atom, while the surrounding regions remain relatively charge-depleted. This result indicates that Cr incorporation induces a local perturbation of the electronic environment within the lattice. Such local electronic redistribution is consistent with the calculated reduction in interfacial energy and the increase in migration barrier, and provides atomic-scale support for the experimentally observed eutectic structure refinement and the retention of nanoscale heterogeneity in the Bi phase. [40]

3.3. Mechanical properties and fracture behavior

Based on our previous research, the addition of Cr and V elements facilitates microstructural reconstruction within the SnBi phase and promotes the formation of a hierarchical structure. To demonstrate the improvement in ductility and toughness achieved by this structure, in-situ tensile experiments were designed and conducted. Initially, to determine the optimal addition levels of Cr and V, alloys with varying amounts of these elements were melted and subjected to tensile testing. The specific compositions are listed in Table 2. Meanwhile, the effects of Cr and V additions on tensile strength and elongation are presented in Figure 7a. Combining the information from the table and the figure, it can be seen that the addition of Cr and V is beneficial for improving both the strength and elongation of the alloy. Notably, the most significant improvements in strength and elongation are achieved with a microalloying

composition of 0.2 wt% Cr and 0.005 wt% V. For convenience, the composition 50Sn49.795Bi0.2Cr0.005V is designated as SBCV.

Table 2 Mechanical properties of CrV alloys with different compositions

Alloy number	Sn (Wt. %)	Bi (Wt. %)	Cr (Wt. %)	V (Wt. %)	Tensile strength (MPa)	Elongation (%)
1	50	Balance	0.1	0.003	78.31	34.01
2	50	Balance	0.3	0.007	79.37	37.81
3	50	Balance	0.2	0.007	81.04	37.99
4	50	Balance	0.3	0.003	78.29	41.01
5	50	Balance	0.1	0.007	80.04	46.35
6	50	Balance	0.3	0.005	81.08	49.36
7	50	Balance	0.2	0.003	79.73	49.44
8	50	Balance	0.1	0.005	79.89	55.44
9	50	Balance	0.2	0.005	79.31	61.52

Fig. 7 displays the typical tensile engineering stress–strain curves and tensile properties of SBCV and Sn-Bi solder alloys. The binary Sn-Bi alloy exhibits limited elongation. The Sn50Bi alloy exhibits an increase in yield strength but a decrease in total elongation relative to the eutectic Sn-Bi alloy, while the further addition of Cr and V substantially enhances the total elongation (61.64±5.08 %) without sacrificing tensile strength (79.47±3.74 MPa).

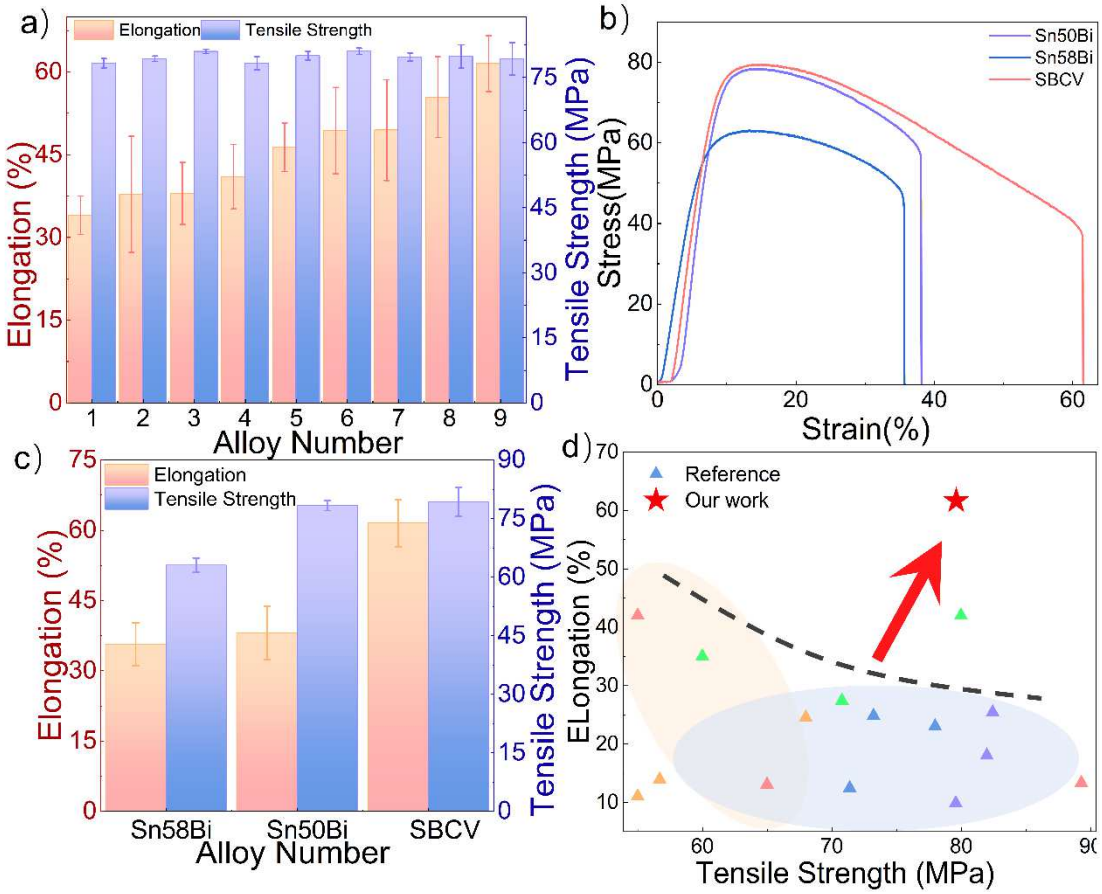


Figure 7. Mechanical performance of the binary Sn-Bi alloys and the microalloyed SBCV alloy. (a) Comparison of elongation and tensile strength of alloys with different Cr and V contents. (b) Stress-strain curves. (c) Comparison of elongation to failure and tensile strength between Sn58Bi, Sn50Bi and SBCV. (d) Mechanical property comparison of the alloy in this work and literature reports[41-46]

In situ SEM observations reveal a progressive and spatially distributed deformation–damage evolution in the SBCV alloy during tensile loading. As shown in Fig. 8a1–f1, the microstructure remains largely intact at the initial stage, whereas local deformation and damage gradually develop with increasing strain. At a strain of approximately 15 %, isolated microcracks are first observed in the microstructure (Fig. 8b1). When the strain increases to approximately 27 %, a macroscopic crack emerges,

accompanied by a pronounced increase in the number of microcracks and a more extensive deformation of the surrounding microstructure (Fig. 8d1). The enlarged views of the β-Sn-rich regions in Fig. 8a2–f2 further clarify the local deformation process. The β-Sn phase starts to deform at the early stage and progressively elongates along the tensile direction with increasing strain, as evidenced by the morphological evolution in Fig. 8a2-c2. Before the formation of the macroscopic crack, the β-Sn-rich regions have already undergone substantial deformation, indicating that they act as the primary strain-accommodating constituents during the early and intermediate stages of loading.

The deformation of the eutectic regions is presented in Fig. 8a3-f3. At relatively low strain, interfacial sliding within the eutectic structure can be identified (Fig. 8b3). With further straining, the Bi-rich regions also become involved in the deformation process, as reflected by the local shape changes and fragmentation-like features shown in Fig. 8c3. These observations indicate that the deformation is not confined to the Sn-rich phase; instead, both Sn-rich and Bi-rich constituents progressively participate in strain accommodation, thereby improving the deformation compatibility within the eutectic structure. At a higher strain of approximately 48%, the Sn and Bi phases undergo simultaneous and severe deformation, while the macroscopic crack propagates along a tortuous path and interacts with numerous microcracks distributed throughout the microstructure (Fig. 8f1–f3).

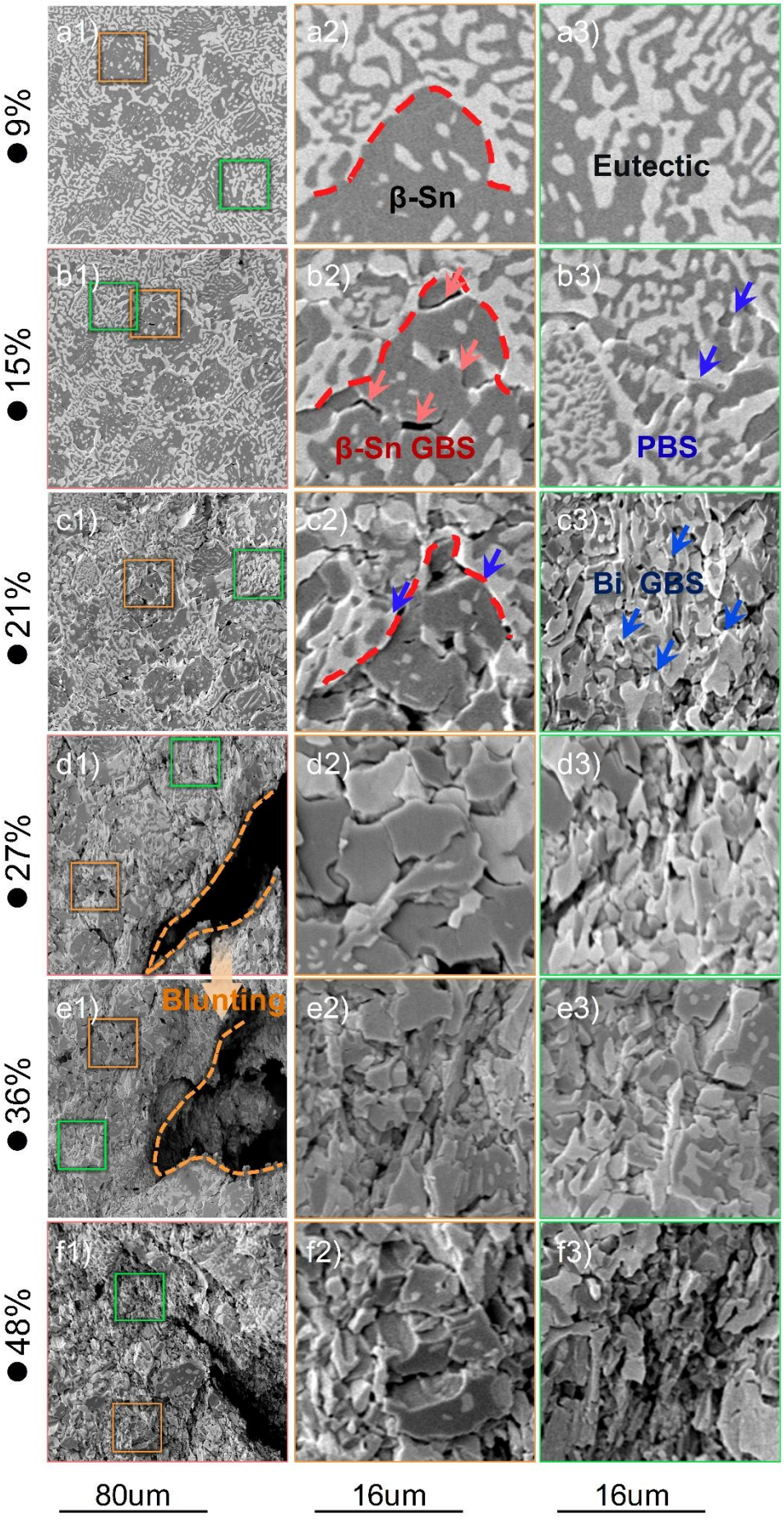

●9%
●15%
●21%
●27%
●36%
●48%
a1)
a2)
a3)
β-Sn
Eutectic
b1)
b2)
b3)
β-Sn GBS
PBS
c1)
c2)
c3)
Bi GBS
d1)
d2)
d3)
e1)
Blunting
e2)
e3)
f1)
f2)
f3)
80um
16um
16um

Figure 8. In situ SEM observations revealing the tensile deformation and fracture behavior of the SBCV alloy at different strain levels: (a) 9%, (b) 15%, (c) 21%, (d) 27%, (e) 36%, and (f) 48%. The subfigures illustrate the microstructural evolution of different regions within the SBCV alloy under increasing strain: (a2)–(f2) correspond to the Sn solid-solution region, and (a3)–(f3) correspond to the eutectic region

A wider-field view of the crack evolution is further provided in Fig. 9. At 15% strain, the alloy exhibits evident deformation, but no macroscopic crack is formed (Fig. 9a). At 27% strain, a macroscopic crack appears, while substantial deformation and numerous microcracks have already developed in other regions of the alloy, as shown in Fig. 8d1–d3. The presence of these distributed microcracks alters the subsequent crack-growth behavior by promoting crack-tip blunting (Fig. 8d1,e1), crack branching (Fig. 9b), and crack deflection (Fig. 9c), thereby delaying the rapid propagation of the macroscopic crack. Therefore, the enhanced plasticity of the SBCV alloy originates from the cooperative deformation of the β-Sn-rich regions and eutectic Sn/Bi constituents, together with a distributed damage-accommodation process that retards catastrophic crack propagation.

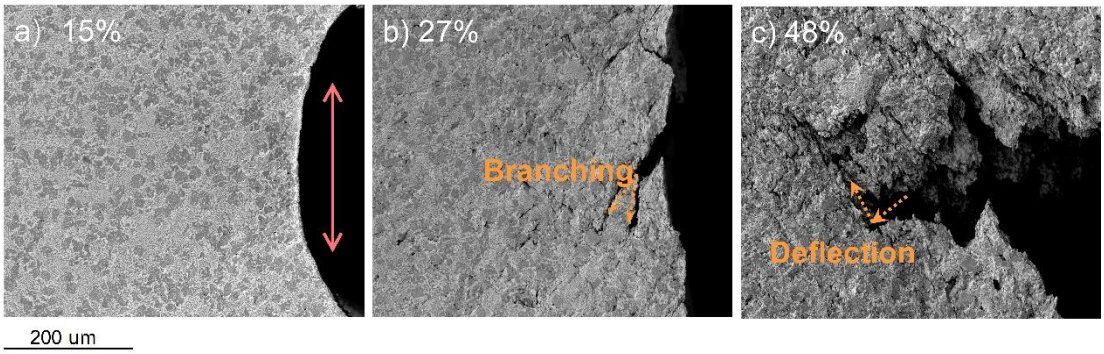


Figure 9. In situ SEM observations at a wider field of view revealing the tensile deformation and

fracture behavior of the SBCV alloy at different strain levels(a) 15%, (b) 27%, (c) 48%

In contrast, in the Sn58Bi and Sn50Bi binary alloys, cracks nucleate and propagate rapidly along phase boundaries, presenting a comparatively straight crack path consistent with cleavage-dominated brittle fracture (Fig. 10). Prior to failure, only minimal plastic deformation is observed within the Bi phase. At a strain of 9%, pronounced interfacial sliding traces appear along the Sn/Bi interfaces (Fig.10 a,d)[18], which becomes more extensive with further deformation (Fig.10 b,e). Unlike in the SBCV alloy, no significant microcrack nucleation is observed within the Bi phase itself. At a strain of 18%, a distinct macroscopic crack has already formed (Fig.10 c,f), while interfacial sliding continues to develop and the contribution from intraphase deformation remains limited.

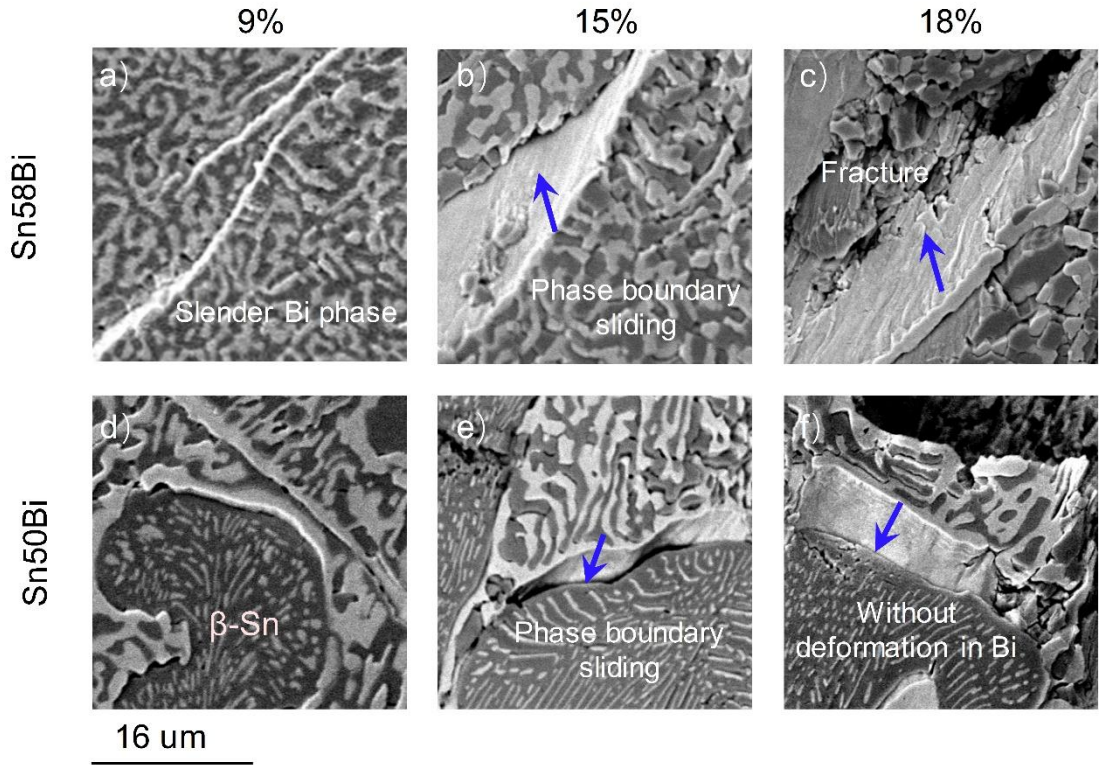


Figure 10. In situ SEM analysis of the (a-c)Sn58Bi and (d-f)Sn50Bi alloys at strain levels of 9%, 15% and 18%

To further understand the correlation between microstructural reconstruction and fracture behavior, phase-field and FEM simulations were performed for uniaxial tension of SnBi and SBCV alloys, with the corresponding results displayed in Fig. 11. The phase-field fracture simulations capture crack propagation along SnBi grain boundaries (Fig. 11a) and crack evolution in the presence of a pre-existing microcrack (Fig. 11b). From the simulation results, the reconstructed microstructure markedly alters the crack evolution pathway, promoting discontinuous crack advance and frequent deflection. To further investigate the influence of microcracks on macroscopic crack behavior, a comparative analysis was conducted between models with multiple microcracks and models without any microcracks. The temporal evolution of stress at the crack tip is plotted in Fig. 10c. In the SBCV alloy, spatially distributed local damage reduces stress concentration at the tip of the dominant crack, thereby suppressing rapid crack propagation. In contrast, in the binary-alloy-like microstructure, the absence of effective stress redistribution leads to rapid stress accumulation at the crack tip, which readily reaches the local damage threshold. Once this threshold is exceeded, the crack propagates directly with minimal deviation, preferentially across Bi-rich regions. This simulated trend is in good agreement with the in situ experimental observations.

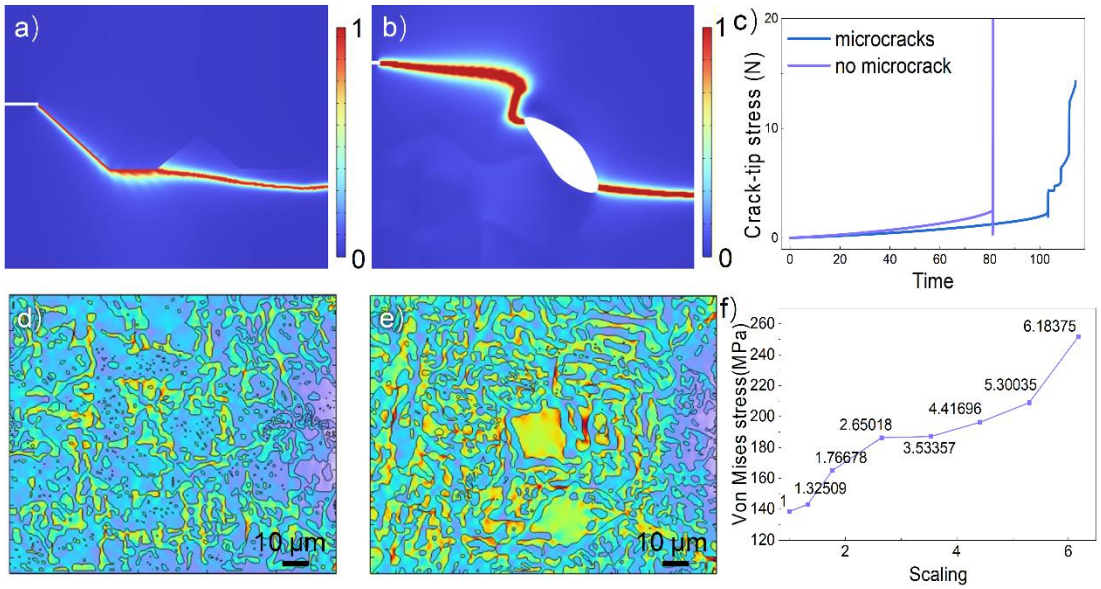


Figure 11. Phase-field and FEM simulation results of SnBi and SBCV alloys. (a) Phase-field simulation of crack propagation at the Sn-Bi interface. (b) Crack propagation in the presence of a pre-existing microcrack. (c) Stress state at the crack tip. (d) Finite element simulation of stress concentration in the SBCV microstructure. (e) FEM simulation of stress concentration in the Sn58Bi microstructure. (f) Stress concentration after magnification (upscaling) of the microstructure

As can be seen in Fig. 10d-e, the microstructural refinement and internal subdivision of the Bi phase contribute to a more homogeneous stress distribution. In the SBCV alloy, stress localization is substantially alleviated, owing to phase refinement and the presence of internal strain-accommodation features within the Bi phase (Fig. 10d). In the Sn-Bi binary alloy, stress concentrates predominantly at Sn/Bi interfaces and around the peripheries of coarse Bi regions（Fig. 11e）. Figure 11f shows the variation of the maximum stress change rate with the scaling factor, obtained from in situ magnification of the SBCV alloy microstructure in Fig. d and stress simulations,

quantitatively characterizing the effect of microstructure size on stress concentration. Before 2.65 times coarsening, stress concentration increases markedly, then enters a plateau with slow growth, followed by a second increase after 5.30 times coarsening. Notably, statistical analysis reveals that, excluding the larger Bi-phase structure in the Sn58Bi alloy, the coarsening degree of the eutectic microstructure is approximately five times that of the SBCV alloy microstructure. Taken together, these simulations provide direct evidence linking microalloying-induced structural reconstruction to enhanced crack propagation resistance.

4. Discussion

4.1. Solid-solution induced interfacial destabilization and substructure formation

A key observation is that Cr and V atoms are dissolved in the Bi lattice without forming detectable secondary phases, while the SBCV alloy exhibits pronounced eutectic refinement together with a substantial increase in LAGBs and dislocation substructures within the Bi phase.

First-principles calculations reveal that Cr and V reduces the Sn/Bi interfacial energy, as shown in Fig. 6b. While this finding does not directly quantify the liquid/solid interfacial energy during eutectic solidification, it unequivocally demonstrates that Cr modifies the interfacial thermodynamics of the Sn/Bi system[47]. This thermodynamic modification is expected to promote interfacial reconstruction and morphological perturbation during coupled eutectic growth. In a eutectic system, front evolution is governed by the interplay of interfacial energy, local solute redistribution, and

curvature-driven effects. Once this interfacial energetic balance is modified, the continuous growth of Bi-phases is more readily interrupted by local front perturbations, interfacial curvature, and repeated adjustments in growth direction. As a consequence, Bi and Sn phases tend to be subdivided into finer structural units during solidification, which is beneficial for mechanical properties. Importantly, this refinement is not merely a reduction in the characteristic scale of the phases, it also involves the formation of abundant low-angle boundaries and dislocation walls within the Bi phase. This is attributed to the fact that the Bi phase experiences repeated local growth interruption and crystallographic reorientation during solidification and the subsequent cooling process.

In addition to modifying interfacial thermodynamics, Cr and V atoms dissolved in Bi phases are also expected to influence boundary migration and defect recovery. Their incorporation introduces local lattice distortion and solute-drag effects[48], thereby reducing the mobility of internal interfaces and suppressing the annihilation of deformation-related substructures during cooling. Under these conditions, local lattice rotations and dislocation rearrangements generated during growth are more readily retained, resulting in the observed low-angle boundaries and dislocation walls[49]. Consequently, the refined eutectic morphology and increased substructure density within the Bi phase should be interpreted as a coupled consequence of growth interruption and solute-stabilized structural retention.

In summary, the dissolution of Cr or V modifies the interfacial energetics of the Bi phase and suppresses boundary migration via solute-drag effects, thereby promoting

eutectic refinement and preserving internal substructures within the Bi phase.

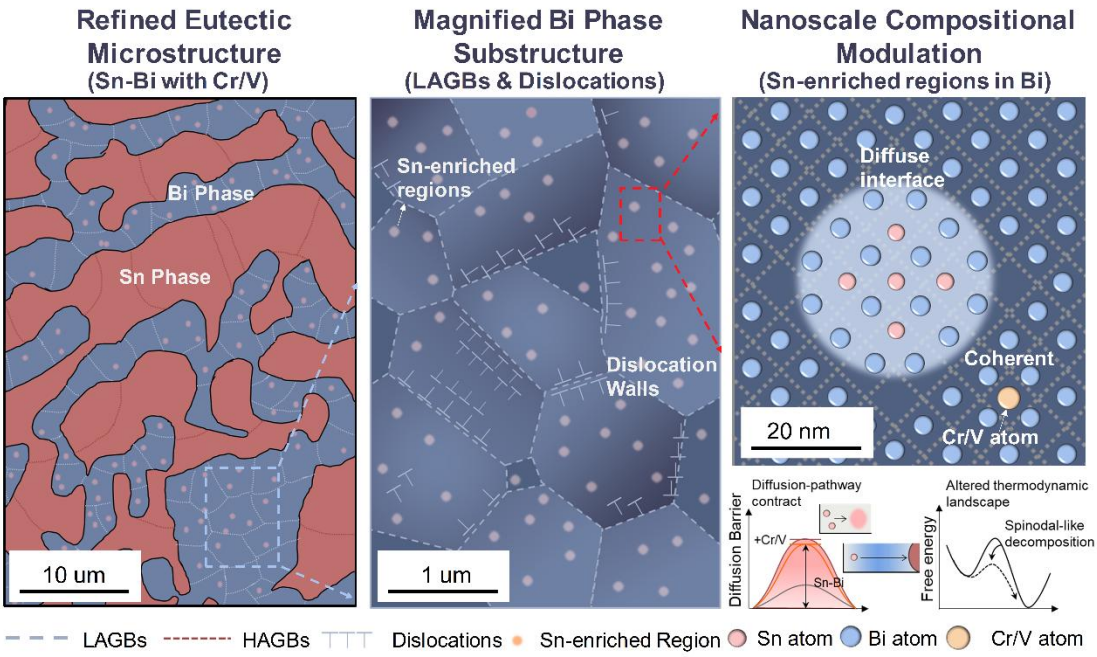


Figure 12. Hierarchical reconstruction of eutectic refinement, Bi substructure, and nanoscale Sn modulation in Cr/V-microalloyed Sn–Bi alloys

4.2. Nanoscale compositional modulation within the Bi phase

Another distinctive feature of the SBCV alloy is the emergence of nanoscale Sn-enriched regions within the Bi phase. As confirmed by the observations in Section 3.1, the addition of Cr and V alters the solidification path of the SBCV alloy—spinodal decomposition leads to the formation of numerous nanoscale Sn-enriched regions within the Bi phase, all of which maintain diffuse interfaces.

Such structural characteristics are consistent with a continuous decomposition pathway. According to the thermodynamic framework of spinodal-like decomposition[39], phase separation is driven by minute compositional fluctuations, proceeding without a detectable nucleation barrier and resulting in diffuse

compositional modulations. Classical precipitation, by contrast, occurs via the nucleation and growth of a new phase. In the present Cr/V-modified alloy, the nanoscale Sn enrichment, together with its coherent character, suggests that the Bi phase undergoes a spinodal-like compositional modulation[50].

Cr and V play a dual role in the formation of nanoscale Sn-enriched regions. Firstly, both elements are uniformly dissolved in the Bi lattice, which are expected to alter the free-energy landscape for phase separation while increasing the energetic penalty associated with local compositional partitioning and coherency strain. On the other hand, first-principles calculations demonstrate that Cr increases the diffusion barrier of Sn in Bi from 0.816 eV to 1.7255 eV, while V raises it from 0.816 eV to 1.7515 eV (Fig. 6c). This substantial increase in migration barrier is expected to strongly suppress long-range diffusion of Sn and the subsequent coarsening of Sn-enriched domains[51]. As a result, once nanoscale compositional fluctuations are established, their evolution into coarse precipitates with sharp interfaces thus becomes kinetically unfavorable, enabling the alloy to retain a metastable nanoscale modulation state[39].

In general, Cr/V microalloying redirects phase separation within the Bi phase toward a coherent, diffuse-interface, nanoscale modulation state. In this context, the distinction between the microalloyed and binary Sn–Bi systems lies in a fundamental change in the phase-separation pathway from classical nucleation and growth to a strain-modulated and kinetically constrained continuous decomposition process.

4.3. Multiscale dual-phase structure-induced toughening mechanism

The refined eutectic structure, nanoscale compositional modulation, and high-

density low-angle substructures collectively constitute a hierarchical internal architecture within the Bi phase, which enhances the strength and ductility of the Sn–Bi-based alloy. In situ observations (Figs. 8-9) demonstrate that the SBCV alloy accommodates tensile deformation through the coordinated participation of β-Sn-rich phases and modified Bi-rich phases. Meanwhile, distributed microcracking induces crack blunting, branching, and deflection, collectively retarding macroscopic crack propagation and enabling enhanced ductility.

4.3.1 Stress redistribution enabled by eutectic refinement

At the mesoscale, eutectic refinement plays a primary role in mitigating stress concentration. In coarse eutectic morphologies, stress tends to localize within individual coarse constituents, generating steep stress gradients near phase boundaries. In contrast, a refined eutectic structure promotes a more homogeneous stress distribution. Finite element simulation results displayed in Fig. 10d-e further confirm this effect, revealing that the refined morphology significantly reduces local stress maxima within the Bi phase. As a result, in the initial stage of tensile deformation, more microstructural features participate in deformation, leading to the formation of microcracks in many regions, which delays the propagation of macroscopic cracks[52].

4.3.2 Subgrain-boundary strengthening and crack deflection

The high density of LAGBs and dislocation walls subdivides the Bi phase into finer crystallographic units. During crack propagation(Fig. 8), these internal substructures force repeated deflection in crack trajectory, as the advancing crack encounters differently oriented regions and internal boundaries[53]. Such crack

deflection increases the effective fracture area and improves the associated energy dissipation. In addition, low-angle boundaries and dislocation walls can serve both as barriers to dislocation motion and as potential sources for dislocation emission.

4.3.3 Nanoscale compositional modulation as local strain-buffering units

The Sn-enriched nanoregions formed by spinodal decomposition within the Bi phase are considered to be crucial for the concurrent improvement in ductility and retention of strength. These compositionally modulated domains introduce local chemical and elastic fluctuations, which can hinder dislocation motion through a spinodal-hardening effect and thereby compensate for possible strength loss associated with enhanced deformability. Meanwhile, owing to their crystallographic coherency with the surrounding Bi matrix, the Sn-enriched regions do not behave as conventional brittle second phases or severe stress concentrators. Instead, they provide nanoscale sites for strain accommodation and promote a more gradual redistribution of local stress[39]. Such a coherent periodic modulation can effectively alleviate strain localization in the Bi phase improve plastic deformation capability. This phenomenon is also consistent with previous reports that spinodal decomposition can help overcome the strength–ductility trade-off[50].

The interplay of these multiscale structural features not only promotes a more homogeneous stress distribution within the alloy under tensile loading, but also renders the crack propagation pathway increasingly tortuous. At the mesoscale, the refined eutectic structure reduces the severity of stress concentration. At the microscale, subgrain boundaries and dislocation structures enhance strain compatibility between

neighboring structural domains, allowing the Bi phase to engage more actively in deformation. Moreover, distributed microdamage within the subdivided Bi phase, along with nanoscale strain-buffering regions, alleviates local stress concentration ahead of the dominant crack tip. These local damage events effectively partition stored elastic energy and reduce the driving force for crack propagation[54]. Consequently, at the macroscopic scale, the dominant crack propagates in a highly tortuous manner and interacts with multiple internal structural features, giving rise to the crack deflection, branching, and local blunting as observed in the in situ experiments.

The net outcome is a substantial increase in strain compatibility between the Sn and Bi phases. The reconstructed Bi phase no longer behaves as a purely brittle constituent, but instead becomes an active participant in deformation.

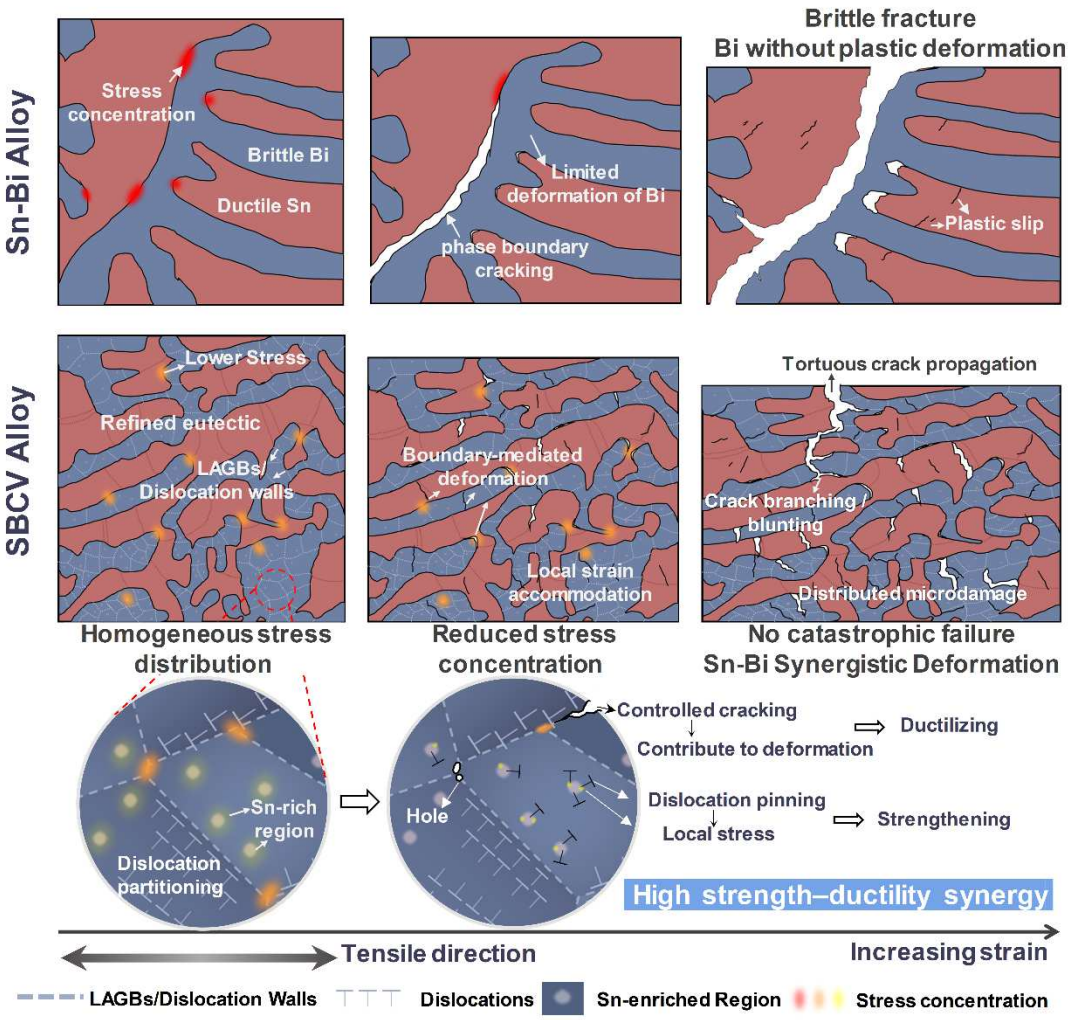


Figure 13. Multiscale mechanisms of solid-solution-induced ductility in Cr/V-microalloyed alloys

Conclusions

In this work, a novel Sn–Bi-based solder alloy with high-strength and high-ductility was developed through trace Cr and V microalloying. The effects of Cr and V on microstructure, Bi-phase reconstruction, deformation behavior and fracture resistance were investigated. The main conclusions are as follows.

The SBCV alloy exhibits an ultimate tensile strength of 79.64 MPa and an elongation of 61.64 %, representing increases of 26.00% and 72.26% over the Sn–Bi alloy. This improvement is attributed to eutectic refinement and enhanced cooperative

deformation between Sn-rich and Bi-rich constituents. The solid solution of Cr and V reduces Sn/Bi interfacial energy, promoting eutectic refinement and suppressing localized stress concentration, thereby enabling uniform strain accommodation and delaying premature fracture.

Trace Cr and V atoms dissolve into the Bi lattice without forming detectable second phases. This solid-solution effect modifies the interfacial state and phase-transformation pathway of the Bi-rich constituent, promoting eutectic refinement and internal crystallographic subdivision within the Bi phase. High-density low-angle grain boundaries and dislocation-wall-like substructures develop inside Bi-rich regions, forming a substructured Bi phase that provides additional strain-accommodation sites, reduces deformation incompatibility between Sn and Bi, and suppresses crack localization.

Within the reconstructed Bi phase, nanoscale Sn-rich regions form coherently with the Bi matrix rather than as coarse precipitates, suggesting a strain-coupled and kinetically constrained composition modulation. These coherent regions buffer local strain, homogenize stress distribution, and impede crack propagation within the Bi phase while avoiding strength deterioration. Thus, nanoscale internal modulation enhances ductility while maintaining high strength.

Together, eutectic refinement, substructure formation, and nanoscale composition modulation construct a multilevel internal architecture within the Bi phase. This hierarchical reconstruction converts the intrinsically brittle Bi-rich constituent from a crack-initiation phase into an active strain resilience unit. This work demonstrates a

microalloying strategy beyond conventional precipitation strengthening, where solid-solution-induced internal reconstruction of the brittle phase offers a new pathway for designing Sn–Bi-based solder alloys with superior strength–ductility synergy.

Author contribution Peng Wu: Experiment, Writing—review & editing, Original draft, Discussion, Ruyu Tian: Original draft, Data curation, Formal analysis. Tao Deng: Experiment, Data curation, Formal analysis. Shuhan Dong: Experiment, Data curation, Formal analysis. Xiaoliang Ji: Writing -review & editing, Discussion. Jianchao Liang: Review & Discussion. Baolei Liu: review & editing. Yanhong Tian: review & editing, Conceptualization.

Funding The authors are grateful for financial support by Science Challenge Project (No. TZ2025004), National Key R&D Program of China (Grant No. 2024YFB3409200) and the Natural Science Foundation of Henan Province (No. 252300421896).

Data availability No datasets were generated or analysed during the current study.

Declarations

Ethical approval Experiments in this paper do not involve any vivo testing on animal subjects, human subjects, or human tissue.

Competing interests The authors declare no competing interests.

References

[1] Tu KN (2011) Reliability challenges in 3D IC packaging technology. Microelectronics Reliability 51.3:517-523. https://doi.org/10.1016/j.microrel.2010.09.031.

[2] Yu Z, Du W, Qiang J, et al (2024) Intermetallic compound evolution and mechanical properties of Sn-0.7Cu-0.1Ni-xZn lead-free solder alloys prepared by directional solidification. Materials Today Communications, 38:107754. https://doi.org/10.1016/j.mtcomm.2023.107754.

[3] Ribas M, Kumar A, Kosuri D, et al (2017) Low temperature soldering using Sn-Bi alloys. Proceedings of SMTA International. 2017: 201-2016. https://doi.org/10.37665/smLCTIJ20680.

[4] Singh P, Palmer L, Wassick T, et al (2025) Planar Geometry Solder Joint Study of Alloying Effects on Sn-Bi Electromigration. 2025 International Conference on Electronics Packaging and iMAPS All Asia Conference (ICEP-IAAC). 2025: 83-84. https://ieeexplore.ieee.org/abstract/document/11003003.

[5] Arvin C, Lim S P, Locker D, et al (2022) Low temperature interconnects in 1st level packaging and its challenges. 2022 International Conference on Electronics Packaging (ICEP). 2022: 7-8. https://ieeexplore.ieee.org/document/9795576.

[6] Ren J, Huang F F, Li A J, et al (2025) Electromigration-induced failure mode of low-temperature Sn–49Bi–1Ag hybrid BGA joint in flip chip package. Journal of Materials Research and Technology 36:9673-9677. https://doi.org/10.1016/j.jmrt.2025.05.197.

[7] Lin S , Nguyen T L, Wu S chang, et al (2014) Effective suppression of interfacial intermetallic compound growth between Sn–58wt.% Bi solders and Cu substrates by minor Ga addition. Journal of Alloys and Compounds 586:319-327. https://doi.org/10.1016/j.jallcom.2013.10.035.

[8] Shen J, Pu Y, Yin H, et al (2014) Effects of minor Cu and Zn additions on the thermal, microstructure and tensile properties of Sn–Bi-based solder alloys. Journal of Alloys and Compounds 614:63-70. https://doi.org/10.1016/j.jallcom.2014.06.015.

[9] Wei Y, Zhao X, Liu Z, et al (2022) Impact of precipitated phases on the microstructure and mechanical properties of eutectic Sn58Bi alloy. Journal of Alloys and Compounds 903:163882. https://doi.org/10.1016/j.jallcom.2022.163882.

[10] Gu, Jian (2015) A novel procedure for failure criteria determination at solder joints under the board level drop test. Materials Testing 57.6:574-579. https://doi.org/10.3139/120.110750.

[11] Yeh, Meng-Kao, and Tzu-Heng Huang (2014) Drop test and finite element analysis of test board. Procedia Engineering 79:238-243. https://doi.org/10.1016/j.proeng.2014.06.337.

[12] Hu X, Chan Y C, Zhang K, et al (2013) Effect of graphene doping on microstructural and mechanical properties of Sn–8Zn–3Bi solder joints together with electromigration analysis. Journal of Alloys and Compounds 580:162-171. https://doi.org/10.1016/j.jallcom.2013.05.124.

[13] Chung S, Kwak J B (2020) Comparative study on reliability and advanced numerical analysis of BGA subjected to product-level drop impact test for portable electronics. Electronics 9(9):1515. https://doi.org/10.3390/electronics9091515.

[14] Fowler H N, Tay S X, Blendell J, et al (2023) Microalloying effects of Sb and Ag on the microstructural evolution of eutectic Sn–Bi alloys. MRS Advances 8(14):763-767. https://doi.org/10.1557/s43580-022-00472-3.

[15] Zhang H, Zhang Q, Song Z (2024) Influences of low In alloying and aging on microstructure and plastic deformation behavior of Sn-58Bi solder. Journal of Materials Science: Materials in Electronics 35(17):1185. https://doi.org/10.1007/s10854-024-13017-1.

[16] Sirpky G, Kraker E, Rosc J, et al (2021) Analysis of Sn-Bi Solders: X-ray Micro Computed Tomography Imaging and Microstructure Characterization in Relation to Properties and Liquid Phase Healing Potential. Materials 14(1):153. https://doi.org/10.3390/ma14010153.

[17] Wu Y, Fowler H N , Weddington N, et al (2024) Effect of Sb and Ag additions on the melting and solidification of Sn-Bi solder alloys. MRS Advances 9(1): 2-6. https://doi.org/10.1557/s43580-023-00619-w.

[18] Cai S, Luo X, Peng J, et al (2021) Deformation mechanism of various Sn-xBi alloys under

tensile tests. Advanced Composites and Hybrid Materials 4(2):379-391. https://doi.org/10.1007/s42114-021-00231-2.

[19] Ye D, Du C, Wu M, et al (2015) Microstructure and mechanical properties of Sn–x Bi solder alloy. Journal of Materials Science: Materials in Electronics 26(6):3629-3637. https://doi.org/10.1007/s10854-015-2880-z.

[20] Hu X J, Sun W, Liao J L, et al (2024) Microstructure evolution and deformation behaviour of Sn-xBi-1Ag Solder alloys: Influences of Bi content. Materials Science and Engineering: A 910:146895. https://doi.org/10.1016/j.msea.2024.146895.

[21] Yang T, Zhao X, Xiong Z, et al (2020) Improvement of microstructure and tensile properties of Sn–Bi–Ag alloy by heterogeneous nucleation of β-Sn on Ag3Sn. Materials Science and Engineering: A 785:139372. https://doi.org/10.1016/j.msea.2020.139372.

[22] Ren G, Collins M N (2016) Alloying influences on low melt temperature SnZn and SnBi solder alloys for electronic interconnections. Journal of Alloys and Compounds 665: 251-260. https://doi.org/10.1016/j.jallcom.2016.01.006.

[23] Kang H, Rajendran S H, Jung J P (2021) Low melting temperature Sn-Bi solder: effect of alloying and nanoparticle addition on the microstructural, thermal, interfacial bonding, and mechanical characteristics. Metals 11(2):364. https://doi.org/10.3390/met11020364.

[24] Hu T, Li S, Li Z, et al (2023) Coupled effect of Ag and In addition on the microstructure and mechanical properties of Sn–Bi lead-free solder alloy. Journal of Materials Research and Technology 26:5902-5909. https://doi.org/10.1016/j.jmrt.2023.08.311.

[25] MOKHTARI O, NISHIKAWA H (2016) Correlation between microstructure and mechanical properties of Sn–Bi–X solders. Materials Science and Engineering: A 651:831-839. https://doi.org/10.1016/j.msea.2015.11.038.

[26] Shen, Yu-An, Chih-Hsiang Liu, and Hao-Zhe Kao (2025) Sn–31Bi–19In alloy: a golden ratio design for exceptional elongation, high strength, and low-temperature soldering. Journal of Materials Research and Technology 37:2727-2739. https://doi.org/10.1016/j.jmrt.2025.06.188.

[27] Shen, Yu-An (2024) Cu–Cu joint with great strength using In/Sn–58Bi hybrid soldering at low temperature (90° C). Journal of Materials Research and Technology 33:4473-4480. https://doi.org/10.1016/j.jmrt.2024.10.108.

[28] Wu X, Wu J, Wang X, et al (2020) Effect of In addition on microstructure and mechanical properties of Sn–40Bi alloys. Journal of Materials Science 55.7:3092-3106. https://doi.org/10.1007/s10853-019-04148-6.

[29] Fowler, Hannah N., et al (2023) Sb additions in near-eutectic Sn-Bi solder decrease planar slip. Journal of Electronic Materials 52.11:7365-7370. https://doi.org/10.1007/s11664-023-10666-6.

[30] Zhou S, Mokhtari O, Nishikawa H (2018) Improvement of Mechanical Properties of Zn-Added Sn58Bi Alloy by Zn Segregation on the Sn-Bi Phase Boundaries During Thermal Aging. 2018 IEEE 68th Electronic Components and Technology Conference (ECTC). 2018: 1899-1905[2025-11-04]. https://doi.org/10.1109/ECTC.2018.00284.

[31] Xu G, Guo F, Wang X, et al (2011) Retarding the electromigration effects to the eutectic SnBi solder joints by micro-sized Ni-particles reinforcement approach. Journal of Alloys and Compounds 509(3):878-884. https://doi.org/10.1016/j.jallcom.2010.09.123.

[32] Feng T, Pati B, Chung K M, et al (2024) Ceramic-to-metal bonding using rare-earth containing Sn–Bi solder. Journal of Materials Science: Materials in Electronics 35(6):369.

https://doi.org/10.1007/s10854-024-12176-5.

[33] SAKUYAMA S, AKAMATSU T, UENISHI K, et al (2009) Effects of a Third Element on Microstructure and Mechanical Properties of Eutectic Sn-Bi Solder. Transactions of The Japan Institute of Electronics Packaging 2(1):98-103. https://doi.org/10.5104/jiepeng.2.98.

[34] Li X, Ma Y, Zhou W, et al (2016) Effects of nanoscale Cu_6Sn_5 particles addition on microstructure and properties of SnBi solder alloys. Materials Science and Engineering: A 684:328-334. https://doi.org/10.1016/j.msea.2016.12.089.

[35] Pan, Qingsong, et al (2021) Gradient cell–structured high-entropy alloy with exceptional strength and ductility. Science 374.6570:984-989. https://doi.org/10.1126/science.abj8114.

[36] Shi, Peijian, et al (2021) Hierarchical crack buffering triples ductility in eutectic herringbone high-entropy alloys. Science 373.6557:912-918. https://doi.org/10.1126/science.abf6986.

[37] Liu X, Liu H, Wu Y, et al (2024) Tailoring phase transformation and precipitation features in a Al21Co19.5Fe9.5Ni50 eutectic high-entropy alloy to achieve different strength-ductility combinations. Journal of Materials Science & Technology 195:111-125. https://doi.org/10.1016/j.jmst.2024.01.044.

[38] Jiang H, Qiao D, Jiao W, et al (2020) Tensile deformation behavior and mechanical properties of a bulk cast Al0.9CoFeNi2 eutectic high-entropy alloy. Journal of Materials Science & Technology 61:119-124. https://doi.org/10.1016/j.jmst.2020.05.053.

[39] Peng, Jian, et al (2022) 2430% Superplastic strain in a eutectic Au-Sn alloy with micrometer-sized grains maintained by spinodal-like decomposition. Acta Materialia 228: 117766. https://doi.org/10.1016/j.actamat.2022.117766.

[40] Yi P, Dong C, Xiao K, et al (2021) Study on corrosion behavior of β-Sn and intermetallic compounds phases in SAC305 alloy by in-situ EC-AFM and first-principles calculation[J/OL]. Corrosion Science, 181:109244. https://doi.org/10.1016/j.corsci.2021.109244.

[41] Wei, Yuhang, et al (2021) Effects of endogenous Al and Zn phases on mechanical properties of Sn58Bi eutectic alloy. Materials Characterization 175: 111089. https://doi.org/10.1016/j.matchar.2021.111089.

[42] Shen, J., Pu, Y., Yin, H., Luo, D., Chen, J (2014). Effects of minor Cu and Zn additions on the thermal, microstructure and tensile properties of Sn–Bi-based solder alloys. Journal of Alloys and Compounds, 614, 63-70. https://doi.org/10.1016/j.jallcom.2014.06.015.

[43] Sakuyama, Seiki, et al (2009) Effects of a third element on microstructure and mechanical properties of eutectic Sn–Bi solder. Transactions of The Japan Institute of Electronics Packaging 2.1:98-103. https://doi.org/10.5104/jiepeng.2.98.

[44] Hu, Tianhan, et al (2023) Coupled effect of Ag and In addition on the microstructure and mechanical properties of Sn–Bi lead-free solder alloy. Journal of Materials Research and Technology 26:5902-5909. https://doi.org/10.1016/j.jmrt.2023.08.311.

[45] Chen, Xu, et al (2015) Effect of In on microstructure, thermodynamic characteristic and mechanical properties of Sn–Bi based lead-free solder. Journal of Alloys and Compounds 633:377-383. https://doi.org/10.1016/j.jallcom.2015.01.219.

[46] Xiao K X, Li C J, Gao P, et al (2023) Significantly enhanced ductility of Sn–57Bi–1Ag alloy induced by microstructure modulation from in addition. Journal of Materials Science: Materials in Electronics 34(20):1551. https://doi.org/10.1007/s10854-023-10946-1.

[47] LEE J G, MORI H. (2004) In-situ observation of alloy phase formation in nanometre-sized particles in the Sn–Bi system. Philosophical Magazine 84(25-26):2675-2686.

https://doi.org/10.1080/14786430410001671421.

[48] Gysakova O V, Galenko P K, Shepelevich V G, et al (2019) Diffusionless (chemically partitionless) crystallization and subsequent decomposition of supersaturated solid solutions in Sn–Bi eutectic alloy. Philosophical Transactions of the Royal Society A: Mathematical, Physical and Engineering Sciences 377(2143):20180204. https://doi.org/10.1098/rsta.2018.0204.

[49] Shang H, Ma Z L, Belyakov S A, et al (2017) Grain refinement of electronic solders: The potential of combining solute with nucleant particles[J]. Journal of Alloys and Compounds, 715:471-485.https://doi.org/10.1016/j.jallcom.2017.04.268.

[50] Park H, Haftlang F, Heo Y, et al (2024) Periodic spinodal decomposition in double–strengthened medium–entropy alloy. Nature Communications 15(1): 5757. https://doi.org/10.1038/s41467-024-50078-6.

[51] DELHAISE A M, CHEN Z, PEROVIC D D (2019) Solid-State Diffusion of Bi in Sn: Effects of Anisotropy, Temperature, and High Diffusivity Pathways. JOM 71(1):133-142. https://doi.org/10.1007/s11837-018-3145-0.

[52] Zhao L, Liu L, Lai Y, et al (2025) Insight into the transition from diffuse microcracking to localized macrocracking in saturated quasi-brittle media: Micro-poromechanics-based approach and analytical solutions. International Journal of Plasticity 195:104508. https://doi.org/10.1016/j.ijplas.2025.104508.

[53] Liu H, He Y, Li M (2025) Promoting strength-ductility synergy through sequential martensitic transformation in a hierarchical heterostructured eutectic high-entropy alloy. International Journal of Plasticity 190:104374. https://doi.org/10.1016/j.ijplas.2025.104374.

[54] Liang Z, Wu J, Liu C, et al (2025) Microcracking in additively manufactured tungsten: Experiment and a nano-micro-macro multiscale model. International Journal of Plasticity 186:104264. https://doi.org/10.1016/j.ijplas.2025.104264.

Supplementary Files

This is a list of supplementary files associated with this preprint. Click to download.

- Supplementarymaterial.docx